

Research Article

Numerical and Experimental Study on Energy Performance of Photovoltaic-Heat Pipe Solar Collector in Northern China

Hongbing Chen, Xilin Chen, Sai Chu, Lei Zhang, and Yaxuan Xiong

School of Environment and Energy Engineering, Beijing University of Civil Engineering and Architecture, Beijing 100044, China

Correspondence should be addressed to Hongbing Chen; chenhongbing@bucea.edu.cn

Received 15 December 2014; Revised 4 March 2015; Accepted 9 March 2015

Academic Editor: Yuehong Su

Copyright © 2015 Hongbing Chen et al. This is an open access article distributed under the Creative Commons Attribution License, which permits unrestricted use, distribution, and reproduction in any medium, provided the original work is properly cited.

Several studies have found that the decrease of photovoltaic (PV) cell temperature would increase the solar-to-electricity conversion efficiency. Water type PV/thermal (PV/T) system was a good choice but it could become freezing in cold areas of Northern China. This paper proposed a simple combination of common-used PV panel and heat pipe, called PV-heat pipe (PV-HP) solar collector, for both electrical and thermal energy generation. A simplified one-dimensional steady state model was developed to study the electrical and thermal performance of the PV-HP solar collector under different solar radiations, water flow rates, and water temperatures at the inlet of manifold. A testing rig was conducted to verify the model and the testing data matched very well with the simulation values. The results indicated that the thermal efficiency could be minus in the afternoon. The thermal and electrical efficiencies decreased linearly as the inlet water temperature and water flow rate increased. The thermal efficiency increased while the electrical efficiency decreased linearly as the solar radiation increased.

1. Introduction

In recent years, photovoltaic technology has been developing quickly. Many studies [1, 2] found that only less than 20% solar energy was converted into electricity, while the rest was converted into heat, which increased photovoltaic (PV) cell temperature. Further studies [3] found that the higher the PV temperature was, the lower the electrical efficiency would be. Every 10°C increase in PV cell temperature led to a decrease of electrical efficiency by about 0.5% [4]. Many researchers tried to increase electrical performance of PV panel by air-cooling [5] or water-cooling [6]. They found that water had better cooling effect than air, but water-cooling had the potential problem of being frozen in cold areas. Therefore, a novel PV-heat pipe (PV-HP) solar collector was proposed as a result.

Pei et al. [7] studied the effect of water flow rates, PV cell covering factor, heat pipe space, and absorber plate coating on the energy performance of the heat pipe PV/T system based on a validated model. He [8] also conducted an annual analysis of heat pipe PV/T system under three different climate areas of China. Zhu et al. [9] investigated the effect of heat pipe space on the energy performance of heat pipe PV/T collector and found that the one with smaller heat pipe

space had better energy performance. Zhang et al. [10, 11] proposed a novel solar PV/loop-heat-pipe heat pump system and investigated its energy performance.

This paper aimed to present a simple combination of commercial PV product with heat pipes for both electrical and thermal energy generation and to investigate the effect of solar radiation, water flow rate, and water temperature at the inlet of manifold (namely, inlet water temperature) on its energy performance in cold areas of Northern China. The structure of PV-HP collector was a little different from those studies. The study might be helpful for the promotion of retrofit of traditional PV system and/or solar water heating system and for easier applications as well.

2. Description of Testing Rig

The testing rig of the PV-HP solar water heating system is shown in Figure 1. It was made up of PV-HP collector, water circulating pump, and water tank. Figure 2 shows a cross-section view of part PV-HP collector. A PV panel with a TPT-EVA-PV-EVA-TPT sandwich structure was fixed onto an aluminum sheet (1mm thick), serving as an absorber plate, through thermal glue for good thermal conductance.



FIGURE 1: The testing rig of the PV-HP solar collector.

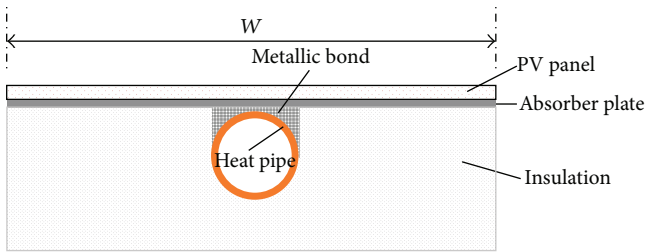


FIGURE 2: Cross-sectional view of part PV-HP collector.

The layer between PV and aluminum sheet was treated as an adhesive layer. Ten heat pipes were bonded to the aluminum sheet, which formed the fins of the heat pipes for the enhancement of heat transfer from PV panel to heat pipes. The heat pipes, 8/7 mm of external/internal diameter for each one, were arranged at equal spacing of 75 mm throughout the panel width. The condensation ends of heat pipes were inserted into a manifold, which was connected to water circulating pump and water tank in series. The edges and back surface of the PV-HP collector were covered with insulation layer to reduce heat loss. The total aperture area and PV cell area were 1.24 m² and 1.17 m², respectively.

The PV panel consisted of 36 PV cells, made of polycrystalline silicon. The PV panel was connected to a rheostat for the testing of power output under various loads and the peak power output was determined at the resistance of 15 Ω. Under the radiation of 1000 W/m² and the ambient temperature of 25°C, the PV panel had an open circuit voltage of 31.0 V and a short circuit current of 8.73 A. The nominal peak power output was 200 W with an electrical efficiency of 16.1%. The list of the testing devices is shown in Table 1.

3. Performance Assessment and Experiment Implementation

3.1. Performance Assessment. The electrical efficiency of the PV panel is given by

$$\eta_c = \frac{E}{GA_p}, \quad (1)$$

TABLE 1: List of testing devices.

Item	Device	Quantity	Location
1	Pyranometer (TBQ-2, China)	1	The same tilt surface beside PV panel
2	Calibrated flow indicator (LZT-15G, China)	1	Water tube after pump
3	Data logger (Agilent 34970A, USA)	1	Indoor workbench
4	PT100 temperature sensor (WZP-01, China)	5	Two at inlet and outlet of manifold and three in water tank

where E is the power output; G is the solar radiation; A_p is the area of PV panel. Consider

$$E = UI, \quad (2)$$

where U is the tested voltage output; I is the electric current.

The thermal efficiency of PV-HP collector is given by

$$\eta_t = \frac{Q}{GA_p}, \quad (3)$$

$$Q = mc(T_o - T_{in}),$$

where Q is the heat obtained by water; m is the water flow rate; c is the specific heat; T_o is the water temperature at the outlet of manifold; T_{in} is the water temperature at the inlet of manifold.

3.2. Experiment Implementation. The testing was carried out at Beijing University of Civil Engineering and Architecture, China, during the period of October 10 to October 27, 2013. The experimental rig was placed on the roof of building number 2 with PV-HP collector exposed to sunshine directly not being in shade. The PV-HP collector was regulated to keep a tilt angle of 30° to simulate the tilt roof-PV installations. The pyranometer was mounted at the same tilt surface beside PV panel to measure the solar radiation on the front surface of PV panel. Two temperature sensors were installed at the inlet and outlet of manifold for measuring water temperature, respectively. The water circulation was driven by water pump and the flow rate was regulated by valve. Three temperature sensors were installed at different depth of water tank to measure water temperature. The average of those three values was considered as the mean water temperature of water tank. The list of testing modes is shown in Table 2.

4. Numerical Models

Zondag et al. [12] built four numerical models for the simulation of PV/T collector: a 3D dynamical model and three steady state models that are 3D, 2D, and 1D. The study showed that the 1D steady state model performed almost as good as the others. Therefore, in order to simplify the simulation process, the 1D steady state model was used for the simulation based on the following assumptions.

TABLE 2: List of testing modes.

Mode	Solar radiation (W/m ²)	Water flow rate (L/min)	Water temp. at the inlet of manifold (°C)
A	650 ± 15	6	20, 23, 26, 29, 32, 35, 38, 41, 44
B	500, 600, 650, 700, 815	6	20 ± 1
C	700 ± 15	5, 7, 9	14 ± 1

- (i) The temperature at each layer of PV-HP collector was well distributed and the geometrical center was selected to be the representative node.
- (ii) The contact resistance between each layer has been neglected.
- (iii) The water pressure drop through the system has been neglected.
- (iv) The heat storage of components was very small and has been neglected.
- (v) For a compact and thin panel design, the losses of the absorbed solar energy to the surrounding were mainly through the front and back panel surfaces, and the edge loss was negligible.

Based on the energy balance analysis of each layer, mathematical models were developed for the numerical simulations on energy performance study. Since the structure of PV-HP collector is similar to the water type PV/T collector of Chow's [13] study, some of the models were employed for the simulation.

The PV-HP solar collector described above can be represented by several nodes. "p" represents the PV panel. "a" is for the surrounding air. "b" is for the thin-plate absorber. "t" is for the metallic bonding between the plate and the heat pipe. "i" is for the insulation layer. "e" is for the evaporation section of heat pipe; "c" is for the condensation section of heat pipe; "w" is for the water in manifold. "s" is for the sky. Figure 3 shows an energy flow diagram of the PV-HP collector.

The heat balance at the PV panel is given by

$$\begin{aligned}
 0 = & GA_{pa}\alpha_p - E + h_{pb}(T_b - T_p)A_{pb} \\
 & + h_{pa}(T_a - T_p)A_{pa} + h_{ps}(T_s - T_p)A_{ps} \\
 & + h_{pt}(T_t - T_p)A_{pt},
 \end{aligned} \quad (4)$$

where G is the solar radiation; A_{pa} is the area of "p" exposed to "a"; α_p is the effective absorptance of "p"; E is the electric power generated; h_{pb} is the heat transfer coefficient between "p" and "b"; A_{pb} is the area between "p" and "b"; h_{pa} is the heat transfer coefficient between "p" and "a"; h_{ps} is the heat transfer coefficient between "p" and "s"; A_{ps} is the area of "p" exposed to "s"; h_{pt} is the heat transfer coefficient between "p" and "t"; A_{pt} is the heat transfer area between "p" and "t";

T_b , T_p , T_a , T_s , and T_t are the temperature of "b", "p", "a", "s", and "t", respectively. Consider

$$\begin{aligned}
 h_{pb} &= \frac{1}{(\delta_p/k_p + \delta_b/k_b)}, \\
 h_{ps} &= \frac{\varepsilon\sigma(T_s^4 - T_p^4)}{(T_s - T_p)},
 \end{aligned} \quad (5)$$

where δ_p and δ_b are the thickness of "p" and "b"; k_p and k_b are the heat conductivity of "p" and "b"; ε is the grey body factor, and σ is the Stefan-Boltzmann constant.

The heat flow from the PV plate to the metallic bond can be considered through two separate paths: (i) through the adhesive layer and then along the absorber plate and (ii) along the PV plate and then through the adhesive layer at the bonding position [13]. Consider

$$\begin{aligned}
 h_{pt}A_{pt} &= \frac{\delta_p L}{(x_p/2k_p + (\delta_{cl}/k_{cl}) \cdot (\delta_p/D_o))}, \\
 x_p &= \frac{W}{4},
 \end{aligned} \quad (6)$$

where δ_p is the thickness of "p"; L is the length of "p"; k_p is the thermal conductivity of "p"; δ_{cl} and k_{cl} are the thickness and thermal conductivity of the adhesive layer; D_o is the outer diameter of heat pipe; W is the heat pipe pitch. Consider

$$h_{pa} = 2.8 + 3u_a, \quad (7)$$

where u_a is the wind velocity. Consider

$$T_s = 0.0552T_a^{1.5}. \quad (8)$$

The heat balance at the absorber plate is given by

$$0 = h_{pb}(T_p - T_b)A_{pb} + h_{bt}(T_t - T_b)A_{bt} + h_{bi}(T_i - T_b)A_{bi}, \quad (9)$$

where h_{bt} is the heat transfer coefficient between "b" and "t"; A_{bt} is the heat transfer area between "b" and "t"; h_{bi} is the heat transfer coefficient between "b" and "i"; A_{bi} is the heat transfer area between "b" and "i"; T_i is the temperature of "i". Consider

$$\begin{aligned}
 h_{bt} &= \frac{2k_b}{x_b}, \\
 x_b &= \frac{(W - D_o)}{4}, \\
 A_{bt} &= \delta_b L,
 \end{aligned} \quad (10)$$

where k_b is the thermal conductivity of "b"; δ_b is the thickness of "b".

$$\begin{aligned}
 h_{bi} &= \frac{2k_i}{\delta_i}, \\
 A_{bi} &= A \left(\frac{(W - D_o)}{W} \right),
 \end{aligned} \quad (11)$$

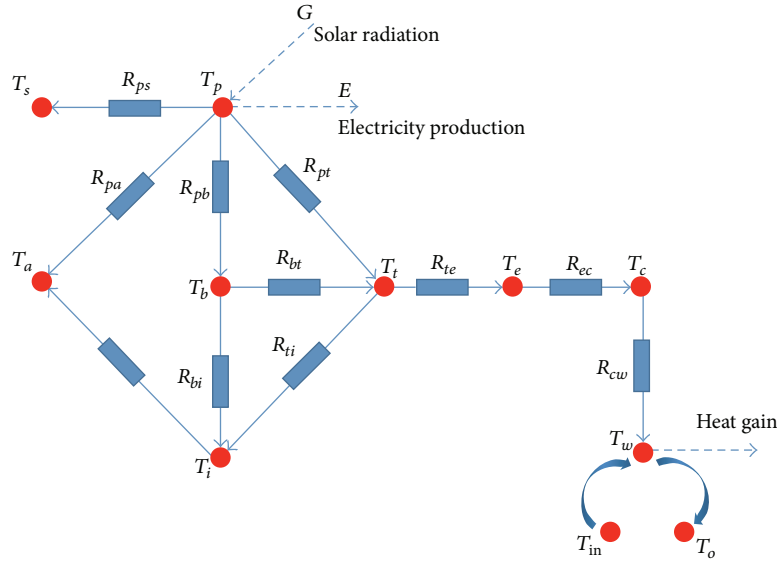


FIGURE 3: Energy flow at PV-HP collector.

where k_i is the thermal conductivity of “ i ” and δ_i is the thickness of “ i .”

The heat balance at the insulation layer is given by

$$0 = h_{bi}(T_b - T_i)A_{bi} + h_{it}(T_t - T_i)A_{it} + h_{ia}(T_a - T_i)A_{ia}, \quad (12)$$

where h_{it} is the heat transfer coefficient between “ i ” and “ t ”; A_{it} is the heat transfer area between “ i ” and “ t ”; h_{ia} is the heat transfer coefficient between “ i ” and the ambient air; A_{ia} is the heat transfer area between “ i ” and “ a .” Consider

$$A_{it} = \left(\frac{\pi}{2} + 1\right)D_oL = 2.571D_oL \quad (13)$$

$$\frac{1}{h_{ia}} = \frac{\delta_i}{2k_i} + \frac{1}{h_{pa}}.$$

The heat balance at the metallic bonding is given by

$$0 = h_{bt}(T_b - T_t)A_{bt} + h_{it}(T_i - T_t)A_{it} + h_{te}(T_e - T_t)A_{te} + h_{pt}(T_p - T_t)A_{pt}, \quad (14)$$

where h_{te} is the heat transfer coefficient between “ t ” and the working medium at “ e .” Heat flow from the metallic bond to the working medium in heat pipe is by means of conduction and convection. Consider

$$\frac{1}{h_{te}A_{te}} = \frac{1}{h_e\pi D_i L} + \frac{1}{TC_{bo}L}. \quad (15)$$

The thermal conduction is determined by the bond conductance given by

$$TC_{bo} = \frac{k_{bo}W_{bo}}{\delta_{bo}}, \quad (16)$$

where k_{bo} is the bond thermal conductivity, δ_{bo} is the bond average thickness, and W_{bo} is the bond width. The convective

heat transfer h_e can be obtained from the Dittus-Boelter equation for fully developed turbulent flow [14],

$$h_e = \text{Nu} \left(\frac{k_e}{D_i}\right), \quad (17)$$

$$\text{Nu} = 0.023\text{Re}^{0.8} \cdot \text{Pr}^{0.4}.$$

For fully developed laminar flow,

$$h_e = \frac{4.364k_e}{D_i}. \quad (18)$$

The heat balance at the evaporation section of heat pipe is given by

$$0 = h_{te}(T_t - T_e)A_{te} + h_{ce}(T_c - T_e)A_{ce}, \quad (19)$$

where h_{ce} is the heat transfer coefficient between the condensation and evaporation sections of the heat pipe; T_c and T_e are the condensation temperature and evaporation temperature of heat pipe, respectively; A_{ce} is the heat transfer area between condensation and evaporation sections. Consider

$$\frac{1}{(h_{ce} \times A_{ce})} = \frac{1}{(h_e \times A_e)} + \frac{1}{(h_c \times A_c)}, \quad (20)$$

where h_c and h_e are the heat transfer coefficients of the condensation and evaporation sections, respectively; A_c and A_e are the heat transfer areas of the condensation and evaporation sections, respectively.

The heat balance at the condensation section of heat pipe is given by

$$0 = h_{ce}(T_c - T_e)A_{ce} + h_{wc}A_{wc}(T_c - T_w), \quad (21)$$

where h_{wc} is the heat convective coefficient between “ w ” and “ c ,” A_{wc} is the heat transfer area between “ w ” and “ c ,” and T_w

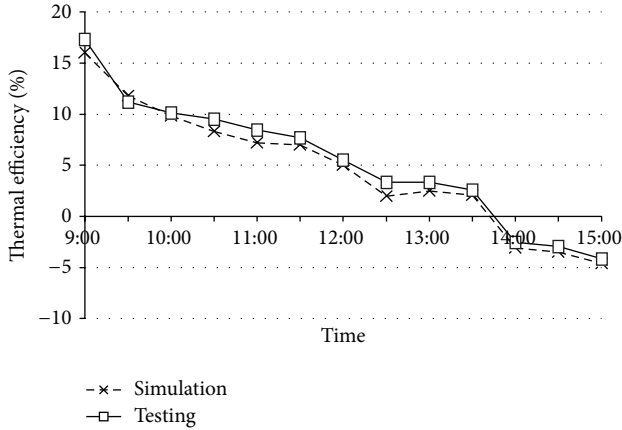


FIGURE 4: Variation of thermal efficiency in the daytime.

is the temperature of “w” ($T_w = (T_o + T_{in})/2$, where T_o and T_{in} are the temperatures of outlet and inlet of the manifold).

The heat balance at circulating water is given by

$$0 = h_{wc}A_{wc}(T_c - T_w) - cm(T_o - T_{in}), \quad (22)$$

where c is the specific heat of water; m is the mass flow of water.

Since the steady-state model was employed for the simulation, it becomes easier to solve those equations. We have the same amount of nonlinear equations and unknown parameters. Matlab was used for programing and solving the system of nonlinear equations.

5. Results and Discussions

5.1. Daily Variation Trend of Electrical and Thermal Efficiencies. Figure 4 shows the variation of thermal efficiency in the daytime. It can be seen from Figure 4 that the thermal efficiency decreases gradually in the daytime, even less than 0% in the afternoon. It is because the water temperature at the inlet of manifold increases with the increasing testing time, and the temperature difference between the circulating water and the condensation end of heat pipe decreases as well, therefore, leading to the decrease of thermal efficiency. As the solar radiation decreases in the afternoon, the water temperature could be higher than the temperature of condensation end, leading to the heat transfer from circulating water to heat pipe, consequently, minus thermal efficiency could occur in the afternoon. The simulation results match quite well with the testing data and the absolute efficiency difference of average thermal efficiency is 0.6%. To avoid the confusion and misunderstanding of the thermal and electrical efficiencies with efficiency difference, all the values of percentage are absolute values in the paper. The thermal efficiency is not as high as expected. That is because the back layer of PV cells is made of white TPT, serving as the electrical insulation of the PV cells. The white TPT back layer is not helpful to enhance the absorption of solar irradiation. Furthermore, the PV-HP collector has a tilt angle of 30°, which is not the best angle for obtaining maximum solar energy in Beijing. The thermal

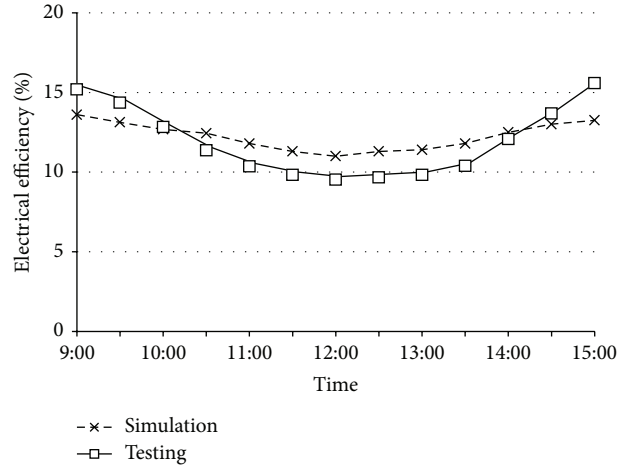


FIGURE 5: Variation of electrical efficiency in the daytime.

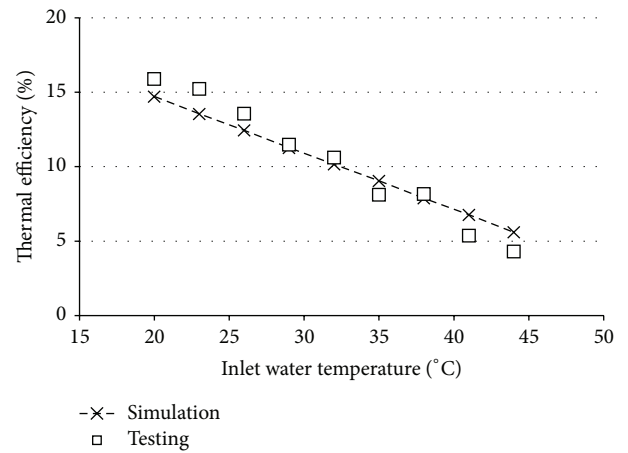


FIGURE 6: Variation of thermal efficiency with inlet water temperature.

efficiency could be improved if the white TPT back layer of PV cells was replaced with black TPT back layer and the tilt angle was increased to the best angle in Beijing.

Figure 5 shows the variation of electrical efficiency in the daytime. It can be seen from Figure 5 that the electrical efficiency of PV panel decreases gradually from the early morning, reaching the minimum at 12:00 and going up in the afternoon. The average tested electrical efficiency is 11.9%, 0.3% lower than the simulation value.

5.2. The Effect of Inlet Water Temperature on Electrical and Thermal Efficiencies. Figure 6 shows the variation of thermal efficiency under different inlet water temperature. It can be seen from Figure 6 that the thermal efficiency decreases sharply and linearly as the inlet water temperature increases, which is because the amount of heat transfer between circulating water and condensation end of heat pipe decreases as the inlet water temperature increases. On average, every 10°C increase of inlet water temperature leads to a thermal

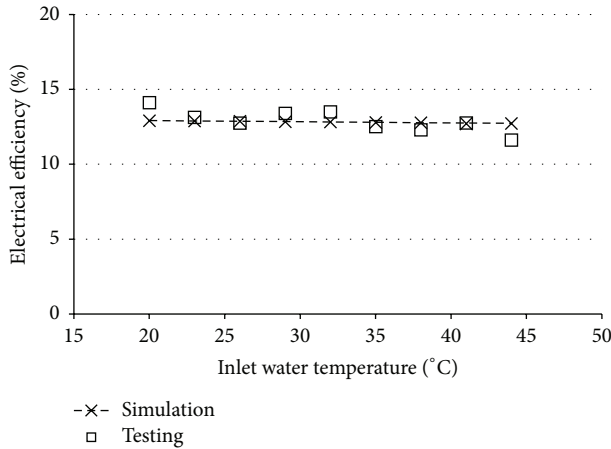


FIGURE 7: Variation of electrical efficiency with inlet water temperature.

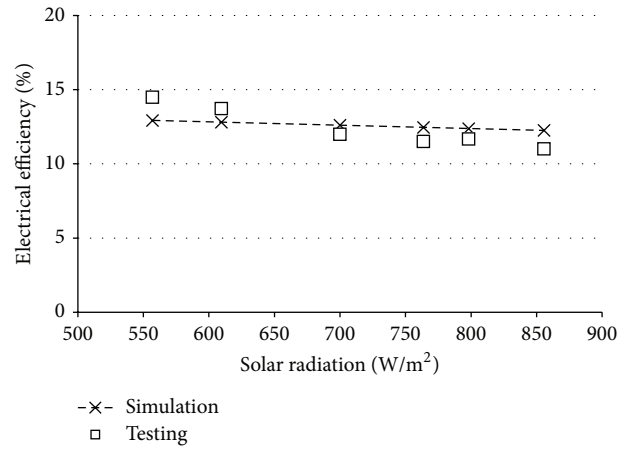


FIGURE 9: Variation of electrical efficiency with solar radiation.

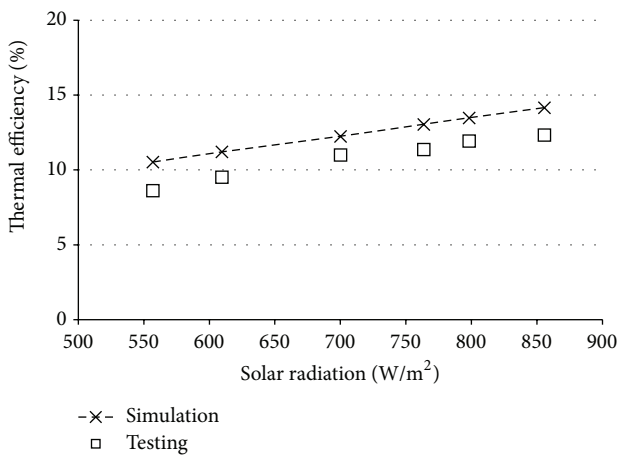


FIGURE 8: Variation of thermal efficiency with solar radiation.

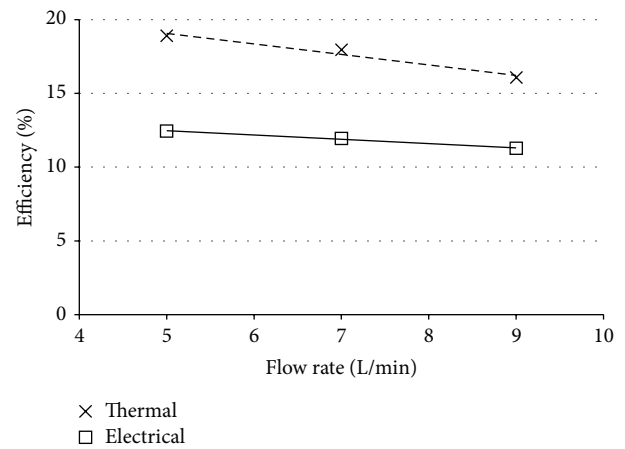


FIGURE 10: Variation of electrical and thermal efficiencies with flow rate.

efficiency decrease by 4.8%. The average thermal efficiency is 10.2% and 10.3% for the simulation and testing, respectively.

Figure 7 shows the variation of electrical efficiency under different inlet water temperature. It can be seen from Figure 7 that the electrical efficiency decreases slightly with the increasing inlet water temperature, which is because high inlet water temperature leads to the poor heat dissipation of PV panel and the increase of PV temperature, resulting in lower electrical efficiency. On average, every 10°C inlet water temperature increase leads to an electrical efficiency decrease by 0.1%. The average electrical efficiency was 12.8% and 12.9% for the simulation and testing, respectively.

5.3. The Effect of Solar Radiation on Electrical and Thermal Efficiencies. Figure 8 shows the variation of thermal efficiency under different solar radiation. It can be seen from Figure 8 that the thermal efficiency increases linearly as the solar radiation increases. On average, every 100 W/m² increase of solar radiation leads to a thermal efficiency increase by 1.2%. The calculating efficiencies are a little higher than the testing ones.

Figure 9 shows the variation of electrical efficiency under different solar radiation. It can be seen from Figure 9 that the electrical efficiency decreases linearly as the solar radiation increases, which is because higher solar radiation leads to more heat in PV panel and higher PV temperature and consequently lower electrical efficiency as well. On average, every 100 W/m² solar radiation increase leads to an electrical efficiency decrease by 0.2%. The average electrical efficiency is 12.6% and 12.4% for the simulation and testing, respectively.

5.4. The Effect of Circulating Water Flow Rate on Electrical and Thermal Efficiencies. Figure 10 shows the variation of thermal and electrical efficiencies under different water flow rates. It can be seen from Figure 10 that the thermal and electrical efficiencies both decrease with the increasing water flow rate. As the water flow rate increases from 5 L/min to 9 L/min, the thermal efficiency decreases from 18.9% to 16.1%, while the electrical efficiency decreases from 12.4% to 11.3%. It is calculated that every 1 L/min increase of water flow rate leads to a thermal efficiency decrease by 0.7% and an electrical efficiency decrease by 0.3% averagely. It is because

higher water flow rate enhances the heat transfer between condensation end of heat pipe and circulating water at the beginning of system operation, and accordingly the water temperature increases quickly. While with the fast increase of water temperature the temperature difference for heat transfer decreases, consequently, the heat transfer is reduced and the thermal efficiency goes down as well, leading to the decrease of electrical efficiency at the same time.

6. Conclusions

This paper presented a study on the electrical and thermal performance of a PV-HP solar collector. Numerical simulation and experiment verification were carried out to investigate the effect of solar radiation, inlet water temperature, and water flow rate on the thermal and electrical efficiencies of the collector. The study could be concluded as follows.

- (1) The thermal efficiency decreases in the daytime and could be minus in the afternoon since the water temperature becomes higher than the PV temperature with the decreasing solar radiation. The electrical efficiency is high in the early morning and later afternoon and reaches the minimum in the noon.
- (2) The thermal efficiency is not as high as expected. It is lower than 20% most of the time due to the white TPT back layer of PV cells and the small tilt angle of PV-HP solar collector. The thermal efficiency could be improved if the white TPT back layer of PV cells was replaced with black TPT back layer and the tilt angle was increased to the best angle in Beijing.
- (3) The thermal and electrical efficiencies decrease linearly as the inlet water temperature and water flow rate increase. The thermal efficiency increases while the electrical efficiency decreases linearly as the solar radiation increases.

Nomenclature

A : Surface area, m^2
 c : Specific heat, $J/kg\ K$
 D : Diameter, m
 E : Power output, W
 G : Solar radiation, W/m^2
 h : Heat transfer coefficient, $W/m^2\ K$
 I : Electric current, A
 k : Thermal conductivity, $W/m\ K$
 L : Length, m
 m : Mass flow rate, kg/s
 Nu : Nusselt number, —
 Pr : Prandtl number, —
 Q : Heat gain, W
 Re : Reynolds number, —
 T : Temperature, $^{\circ}C$
 TC : Thermal conductance, $W/m\ K$
 U : Voltage, V
 u : Wind velocity, m/s

W : Heat pipe pitch or width, m
 x : Distance, m .

Greek

α : Effective absorptance, —
 β : Absorptance, —
 δ : Thickness, m
 ε : Grey body factor, —
 η_t : Thermal efficiency, —
 η_e : Electrical efficiency, —
 λ : Heat conductive coefficient, $W/m\ K$
 σ : Stefan-Boltzmann constant, $5.67 \times 10^{-8}\ W/m^2\ K^4$
 τ : Transmittance, —.

Subscripts

a : Surrounding air
 b : Thin-plate bonding
 bo : Bond
 c : Condensation section of heat pipe; PV cells
 cl : Combined layer
 e : Evaporation section of heat pipe
 i : Insulation layer
 in : Inlet
 o : Outlet
 p : PV panel
 s : Sky
 t : Metallic bonding
 w : Water.

Conflict of Interests

The authors state that there is not any conflict of interests related to this paper.


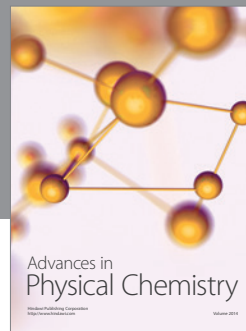
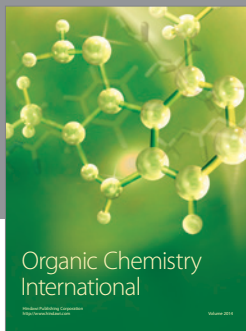
Acknowledgments

The work of this paper is fully supported by Project of National Natural Science Foundation of China (51206004), Funding Project for New Star of Scientific and Technical Research of Beijing (2011029), The Importation and Development of High-Caliber Talents Project of Beijing Municipal Institutions (CIT&TCD201304067), and Beijing Municipal Key Lab of HVAC (KF201004).

References

- [1] E. Skoplaki and J. A. Palyvos, "On the temperature dependence of photovoltaic module electrical performance: a review of efficiency/power correlations," *Solar Energy*, vol. 83, no. 5, pp. 614–624, 2009.
- [2] Y. B. Assoa, C. Menezes, G. Fraisse, R. Yezou, and J. Brau, "Study of a new concept of photovoltaic-thermal hybrid collector," *Solar Energy*, vol. 81, no. 9, pp. 1132–1143, 2007.
- [3] H. A. Zondag, "Flat-plate PV-thermal collectors and systems: a review," *Renewable and Sustainable Energy Reviews*, vol. 12, no. 4, pp. 891–959, 2008.

- [4] T. Yamawaki, S. Mizukami, T. Masui, and H. Takahashi, "Experimental investigation on generated power of amorphous PV module for roof azimuth," *Solar Energy Materials and Solar Cells*, vol. 67, no. 1–4, pp. 369–377, 2001.
- [5] A. Shahsavari, M. Salmanzadeh, M. Ameri, and P. Talebizadeh, "Energy saving in buildings by using the exhaust and ventilation air for cooling of photovoltaic panels," *Energy and Buildings*, vol. 43, no. 9, pp. 2219–2226, 2011.
- [6] S. Odeh and M. Behnia, "Improving photovoltaic module efficiency using water cooling," *Heat Transfer Engineering*, vol. 30, no. 6, pp. 499–505, 2009.
- [7] G. Pei, H. D. Fu, H. J. Zhu, and J. Ji, "Performance study and parametric analysis of a novel heat pipe PV/T system," *Energy*, vol. 37, no. 1, pp. 384–395, 2012.
- [8] G. Pei, H. D. Fu, J. Ji, T. T. Chow, and T. Zhang, "Annual analysis of heat pipe PV/T systems for domestic hot water and electricity production," *Energy Conversion and Management*, vol. 56, pp. 8–21, 2012.
- [9] H. J. Zhu, G. Pei, H. D. Fu, T. Zhang, and J. Ji, "Comparative research between two different heat pipe spaces PV/T Systems," *Acta Energetica Sinica*, vol. 34, no. 7, pp. 1172–1176, 2013.
- [10] X. X. Zhang, X. D. Zhao, J. C. Shen, J. Xu, and X. Yu, "Dynamic performance of a novel solar photovoltaic/loop-heat-pipe heat pump system," *Applied Energy*, vol. 114, pp. 335–352, 2014.
- [11] X. X. Zhang, J. C. Shen, P. Xu et al., "Socio-economic performance of a novel solar photovoltaic/loop-heat-pipe heat pump water heating system in three different climatic regions," *Applied Energy*, vol. 135, no. 1, pp. 20–34, 2014.
- [12] H. A. Zondag, D. W. de Vries, W. G. J. van Helden, R. J. C. van Zolingen, and A. A. van Steenhoven, "The yield of different combined PV-thermal collector designs," *Solar Energy*, vol. 74, no. 3, pp. 253–269, 2003.
- [13] T. T. Chow, "Performance analysis of photovoltaic-thermal collector by explicit dynamic model," *Solar Energy*, vol. 75, no. 2, pp. 143–152, 2003.
- [14] J. A. Duffie and W. A. Beckman, *Solar Engineering of Thermal Processes*, John Wiley & Sons, New York, NY, USA, 2nd edition, 2006.



Hindawi

Submit your manuscripts at
<http://www.hindawi.com>

